Controlled Dispersion and Setting of Cellulose Nanofibril (CNF) - Carboxymethyl Cellulose (CMC) Pastes

Sami Miguel El Awad Azrak (sami_azrak@hotmail.com)
Purdue University College of Engineering https://orcid.org/0000-0002-6384-7212
Jared Gohl
Purdue University College of Engineering
Robert Moon
USDA Forest Products Laboratory
Gregory Schueneman
USDA Forest Products Laboratory
Chelsea Davis
Purdue University College of Engineering
Jeffrey Youngblood
Purdue University College of Engineering

Research Article

Keywords: Cellulose nanofibrils, carboxymethyl cellulose, carbodiimide, polyamide epichlorohydrin, polyamine epichlorohydrin, redispersion

Posted Date: April 19th, 2021

DOI: https://doi.org/10.21203/rs.3.rs-376512/v1

Version of Record: A version of this preprint was published at Cellulose on July 27th, 2021. See the published version at https://doi.org/10.1007/s10570-021-04081-5.

Abstract

This work investigated the redispersion and setting behavior of highly loaded (~18 wt.% solids in water) pastes of cellulose nanofibrils (CNFs) with carboxymethyl cellulose (CMC). A single-screw extruder was used to continuously process CNF+CMC pastes into cord. The adsorption of CMC onto the CNF fibrils was assessed through zeta potential and titration which revealed a surface charge change of ~61 % from -36.8 mV and 0.094 mmol/g COOH for pure CNF to -58.1 mV and 0.166 mmol/g COOH for CNF+CMC with a CMC degree of substitution of 0.9. Dried CNF with adsorbed CMC was found to be fully redispersible in water and re-extruded back into a cord without any difficulties. On the other hand, chemical treatment with hydrochloric acid, a carbodiimide crosslinker, or two wet strength enhancers (polyamide epichlorohydrin and polyamine epichlorohydrin) completely suppressed the dispersibility previously observed for dried-untreated CNF+CMC. Turbidity was used to quantify the level of redispersion or setting achieved by the untreated and chemically treated CNF+CMC in both water and a strong alkaline solution (0.1 M NaOH). Depending on the chemical treatment used, FTIR analysis revealed the presence of ester, N-acyl urea, and anhydride absorption bands which were attributed to newly formed linkages between CNF fibrils, possibly explaining the suppressed redispersion behavior. Water uptake of the differently treated and dried CNF+CMC materials agreed with both turbidity and FTIR results.

Introduction

Cellulose nanomaterials (CNMs) are abundant, sustainable, biodegradable, and can be produced at an industrial scale (up to 1000 kg/day dry equivalent) at relatively low costs(Moon et al. 2011; Axelsson et al. 2012; Assis et al. 2018; Rol et al. 2020). Due to these facts, CNMs are a natural fit to the growing concept of a circular economy(Kaur et al. 2018; Shogren et al. 2019). Depending on the nanoparticle isolation process, source material, and pretreatments used, different types of CNMs are possible each with its own unique characteristics and properties(Moon et al. 2011, 2016; Foster et al. 2018). The current study focuses on cellulose nanofibrils (CNFs) which are typically produced by mechanically fibrillating wood pulp. In contrast to other CNMs, CNFs are flexible nanoparticles with a lower crystalline content (51 % to 69 % crystallinity), higher aspect ratios (up to 500), and a strong tendency to form tangled/aggregated networks as well as have little to no charge(Moon et al. 2011, 2016). Current and potential applications for CNFs include foams, gels, coatings, as well as a reinforcement material in composite fibers and films or as self-standing neat isotropic films (“nanopaper”) and laminated sheets, to name just a few(Sehaqui et al. 2010; Zhang et al. 2013; Clarkson et al. 2019, 2020b, a; El Awad Azrak et al. 2019).

Unlike CNFs which are produced by mechanical fibrillation, carboxymethyl cellulose (CMC) is an ionic ether derived from cellulose prepared from the esterification reaction between alkaline cellulose and monochloroacetic acid(Murray 2009; Lin et al. 2013). This reaction causes the substitution of some of the hydroxyl groups in the glucose repeat unit for negatively charged carboxymethyl groups ($-CH_2-COO^-$) (Murray 2009). The average number of hydroxyl groups substituted per glucose unit is referred to as the

one would mean that on average one out of three -OH

groups were replaced. Owing to its nontoxic nature and its ability to fully dissolve in water, CMC has found uses in the food, cosmetic, and pharmaceutical industries as a highly effective thickener, viscosifier, gelling agent, and rheological modifier(Williams and Phillips 2009; Feddersen and Thorp 2012). CMC has even been reported to significantly reduce the yield stress by 60–80 % of highly loaded lignocellulosic biomass pastes (up to 25 wt.% solids) from corn stover which, in turn, facilitated their processing for use as plausible liquid fuel alternatives(Samaniuk et al. 2012, 2015). More recently, CMC has shown to be an excellent water-soluble processing aid to highly loaded CNF pastes (up to 25 wt.% solids) and in turn allowed for continuous extrusion of CNF sheets without reducing the mechanical performance(El Awad Azrak et al. 2020).

CMC's effectiveness as a processing aid in CNF systems could be tied to its ability to adsorb irreversibly to the surface of the fibrils(Butchosa and Zhou 2014). This adsorption occurs due to the attachment of unsubstituted CMC cellulose units onto the surface of exposed cellulose chains on CNF fibrils. In the wet state (i.e., suspension), the adsorbed CMC carboxylates reduce fibril-fibril contacts and fibril-fibril friction and entanglements(Schmid and Klingenberg 2000). A reduction in apparent viscosity has been reported in highly loaded CNF + CMC and corn-stover + CMC pastes which agrees with the stated theories(Samaniuk et al. 2012; El Awad Azrak et al. 2020). This absorption behavior has also been observed for low solids (1–3 wt.%) pulp systems that contain CMC as a wet end additive(Beghello and Lindström 1998; Watanabe et al. 2004; Yan et al. 2006; Liimatainen et al. 2009). Furthermore, fully dried CNF with adsorbed CMC have been reported to be redispersible possibly due to the reduced number of hydrogen bonds formed and the added negative surface charges which facilitates swelling(Butchosa and Zhou 2014).

Considering that most CNMs processed today contain no more than 30 wt.% solids, the ability of a CNM system, like that of CNF, to fully redisperse after being dried can significantly aid their commercialization by reducing the costs associated with transportation. In this way, CNFs can be transported in the dry state and redispersed at the manufacturing plant to the desired solids concentration for further processing. Additionally, understanding the possible methods or pretreatments that will allow for a semi-permanent setting of CNFs after being processed into the desired shape (e.g., clamshells, cups, sheets, etc.) can in turn expand their possible uses in the dry state by reducing their susceptibility to humid conditions. For these reasons, understanding and having the ability to control the redispersion and setting behavior of CNFs becomes very important.

In this paper highly loaded (~ 18 wt.% solids) CNF + CMC pastes were prepared using a high shear Banbury mixer. Subsequently, a single-screw extruder was used to form the prepared pastes into wet filament/cord and proved to be an effective bulk processing technique for CNF + CMC. Three different CMC degrees of substitution were evaluated (0.7, 0.9, and 1.2), all with the same molecular weight of 250,000. Zeta potential and titration were used to quantify the surface charge (mV) and the amount of active carboxylic groups (mmol/g) adsorbed on CNF fibrils, respectively. The re-dispersibility of the dry and pelletized CNF + CMC pastes was qualitatively assessed by remixing and re-extrusion and [illegible]easurements both in DI water and in an alkaline solution (0.1

M NaOH). To investigate the possible setting of CNF + CMC, different chemical treatments were assessed including two popular waterborne wet strength enhancers (polyamide epichlorohydrin (PAE) and polyamine epichlorohydrin (PAmE)) and a waterborne carbodiimide crosslinker (CDI). Treatment with hydrochloric acid (HCl), the multivalent cationic salt calcium chloride ($CaCl_2$) and the polycationic polymer polyethyleneimine (PEI) was also investigated. Similarly, the effectiveness of the setting behavior of the different chemical treatments was assessed through turbidity. Lastly, FTIR was used to elucidate the possible mechanisms behind the suppressed redispersion behavior observed for each chemical treatment.

Experimental Section/methods

Materials

Hydrochloric acid (HCl) solution at 37 %, calcium chloride ($CaCl_2$) powder, and branched polyethyleneimine (PEI, M_W ~800) were procured from Sigma-Aldrich. Standardized 0.1 M NaOH solution was purchased from Fisher Scientific. Picassian® XL 702, a waterborne polycarbodiimide (CDI) crosslinker with a solids content of 40%, was kindly provided by Stahl Polymers. Two waterborne crosslinking resins of polyamide epichlorohydrin (Polycup™ 9200, Lot#0002475278, 20 % solids, PAE) and polyamine epichlorohydrin (Polycup™ 7360A, Lot# 2459303, 38 % solids, PAmE), were kindly supplied by Solenis LLC. Powders of carboxymethyl cellulose sodium salt (CMC-Na) with three different degrees of substitution (D.S.) of 0.7, 0.9, and 1.2 and with a molecular weight of Mw = 250,000 (Lot# MKCK7917, Lot# MKCF4819, and Lot# MKCF8509) were purchased from Sigma Aldrich. Mechanically fibrillated CNFs were procured from University of Maine, Orono, ME, USA at a concentration of ~ 23.5 wt.% solids in water (Batch #122, 90% fines retained). The process of isolating this specific type of CNFs is explained in detail by C.A. de Assis et al(Assis et al. 2018). Two TEM images of the mechanically fibrillated CNF used are shown Figure S1. Purified water was produced using a Barnstead system and used for all experiments. Unless otherwise stated, solutions of HCl, $CaCl_2$, PEI, PAE, and PAmE were prepared with water.

Preparation of Highly Loaded CNF + CMC Pastes

The preparation of highly loaded CNF + CMC pastes has been explained in detail in a previous publication(El Awad Azrak et al. 2020). In brief, 52 g of CNF (at ~ 23.5 wt.%) was loaded into a high shear torque mixer (Plasti-Corder PL 2100 Electronic Torque Rheometer, C. W. Brabender, South Hackensack, NJ) equipped with Banbury type mixing blades and mixed at 55°C and 120 rpm. While the CNF was being mixed, CMC powder was gradually added until reaching a dry weight CMC:CNF ratio of 0.1:1. Water was added to adjust the paste's solids concentration to ~ 18 wt.%. The paste was mixed until complete CMC incorporation, which was signaled by a constant toque reading/plateau. The entire mixing process took on average less than 40 min and yielded approximately 66 g of wet CNF + CMC paste. This mixing process was repeated for each of the different CMC degrees of substitution (0.7, 0.9, and 1.2). The refrigerator to avoid any microbiological growth and used as

quickly as possible. It is important to note that the word “paste” is used throughout the report to refer to these highly loaded CNF + CMC mixtures. The word “suspension” is used to refer to dilute suspensions prepared from the wet or dried pastes, respectively.

CNF + CMC Filament/Cord Processing

The prepared CNF + CMC pastes were extruded using a Brabender torque rheometer (ATR) with an attached single-screw extruder unit (L/D = 25, barrel diameter of 1.9 cm, and a conventional 3:1 compression screw). A filament head attachment with a 2 mm nozzle was used. Extrusion was carried out at 25°C and at a screw speed of 10 rpm. The filament/cord was collected using a cardboard roll.

Chemical Treatment

The extruded wet CNF + CMC cords were cut into ~ 100 mm long segments with an approximate wet diameter of 2 mm (see Figure S2a). Treatment solutions of 0.1 M HCl, 0.1 M $CaCl_2$, 10 % PEI, 10 % PAE, and 10 % PAmE were freshly prepared. The still wet cord segments were carefully submerged into the different treatment solutions, respectively. Treatment time, solution concentration, and drying/curing temperature were optimized through preliminary experimental trials with HCl and assumed to also apply for $CaCl_2$ (see Figure S3, Figure S4, and Figure S5). It was determined that a concentration of 0.1 M was ideal to retain the cord’s dimensions while a soak time of 20 min allowed for the treatment to penetrate a distance of 2 mm (i.e., the cord’s diameter). After the respective treatment, excess solution was drained off and the cord segments were oven dried at 70 ºC for 1 h, to avoid any oxidation or browning. For treatment with PEI, PAE, and PAmE, the cord segments were cured in the oven at 70°C for PEI, and 85°C or 25°C for PAE and PAmE (per supplier recommendations). Due to CDI’s reactivity at room temperature conditions and the required acidic conditions for correct activation, the treatment process was slightly adjusted. CDI was mixed directly into the CNF + CMC paste at a dry weight ratio of CMC:CDI of 1:1. Subsequently, the CNF + CMC + CDI cord segments were submerged for 20 minutes in 0.1 M HCl and cured at 70°C or 25°C. Lastly, oven dried CNF + CMC cord segment without any treatment, termed “untreated” were also prepared and dried at 70°C for 1 h.

Pelletization

For all treatments and degrees of substitution, the dried and cured CNF + CMC cords were cut by hand using scissors into pellets with an approximate length of ~ 1 mm. Longer untreated CNF + CMC cords were pelletized using a commercial pelletizer (Davis Standard, Pawcatuck, CT, Model PK-102) running at 30 rpm for the rehydration and remixing analysis.

Zeta Potential

The prepared CNF + CMC pastes (D.S. = 0.7, 0.9, and 1.2 all at ~ 18 wt.%) were diluted to 1 wt.%. CNFs adsorbed with CMC were precipitated by centrifugation (10,000 RFC) with any unbound CMC remaining in the supernatant. The supernatant was discarded and the CNF fibrils were resuspended by shear mixing in purified water. This process was repeated 3 times. Subsequently, the washed suspensions were further [illegible]%. Zeta potential measurements were carried out using a

Zetasizer Nano ZS (Malvern Panalytical) and disposable folded capillary cells (Model: DTS1070). The viscosity of the suspensions was not measured but was assumed to be that of water due to the low solids concentration. The pH of all the suspensions was measured to be 6.6 (HANNA® Instruments). Eight measurements were recorded, and the average was reported along with ± STD error bars. Quality criteria were met for all suspensions analyzed, yet the count rate varied for pure CNF suspensions.

Titration

From the ~ 1 wt.% CNF + CMC suspensions prepared for zeta potential analysis, 5 mL were added to 250 mL beakers and diluted with 50 mL of deionized water. 500 mL of 0.1 M HCl was added to fully protonate the carboxylic acid groups on the CNFs. The resulting mixture was titrated with 5 mM NaOH solution. The pH was monitored using an Oakton Acorn pH meter. Representative titration curves (pH verses titrant volume) can be seen in Figure S6. The volume between the two inflection points on the curve was used to calculate the amount of COOH present on the nanofibers.

Turbidity

0.17 g of the treated or untreated CNF + CMC pellets were added into a scintillation vial followed by 17 mL of purified water or 17 mL of a 0.1 M NaOH solution (i.e., a target concentration of 1 wt.% solids). The pellets were stirrer in solution for 24 h at 1000 rpm and 25 ºC. This was repeated for each different degree of substitution and treatment type. Additionally, 1 wt.% never-dried CNF + CMC and pure CNF suspensions were prepared as control groups. Following stirring, 100 mL of the supernatant, with an unknown solids concentration of redispersed CNFs, was diluted with an additional 17 mL of purified water. Dilution was performed to be in the most accurate reading range of the turbidity meter. The dilute suspensions were analyzed using a nephelometric turbidimeter (Vernier®, Beaverton, OR) consisting of a 90º photodiode detector and an 890 nm infrared LED light source. The turbidity meter was calibrated using a 100 NTU Formazin standard and DI water (i.e., 0 NTU) in a glass cuvette. Before collection, a 10 mm stir bar was added to the sample glass cuvette, and the turbidity meter was placed on top of a stir plate. Turbidity was continuously collected every 0.5 s for 650 s while the suspension was being stirred at 400 rpm. Six measurements were carried out per sample group with a fresh diluted sample loaded for every measurement. The average between all 6 measurements is reported along with ± STD error bars as stated under the figures, respectively.

FTIR-ATR

Treated and untreated CNF + CMC pellets, CMC powder (D.S. = 0.7), and a pure cast CNF film were conditioned in a vacuum oven for 24 h at room temperature. The samples were placed in direct contact with the ATR crystal and a 550 cm^{-1} to 4000 cm^{-1} spectra was captured using an FTIR-ATR system (PerkinElmer) with a resolution of 4 cm^{-1}. 20 sample scans were collected, and background subtraction was performed, respectively. Baseline correction was applied to all the spectra for fair comparison.

Scanning Electron Microscopy (SEM)

~ 25 mm long dry segments of untreated CNF + CMC cord were secured to a conductive aluminum stub with carbon tape and then sputter coated (SPI sputter coater) with a platinum-gold target for 60 s. No polishing or sanding was used. The samples were imaged using a Quanta 650 FEG field emission electron microscope at 3 KeV and a spot size of 5. The working distance varied from 39–41 mm to achieve the highest resolution.

Results And Discussion

CNF + CMC Bulk Processing and Pelletizing

Extrusion-based processes are one of the most versatile, commercially available, and easily scalable processing methods used for current commodity polymers. For these reasons, a single-screw extruder was employed to continuously extrude the highly loaded (~ 18 wt.%) CNF + CMC pastes. Results show that wet filament with a diameter of ~ 2 mm (~ 1 mm dry) can be successfully processed without any restrictions on its final length. The extrusion and collection process are shown in Video S1. The extruded cord was collected and oven dried on a carboard roll as shown in Fig. 1a and Fig. 1b. Constrained drying was necessary for the CNF + CMC cord to retain its shape and avoid shrinking/warping (see Fig. 1c verses Figure S7). Following drying, the cord was easily pelletized by using a commercial pelletizer running at 30 rpm as shown in Fig. 1d and Video S2. The processed CNF + CMC pellets had an average length of 6.73 ± 2.5 mm. Roughly 10 g of dry cord were processed and presented in Fig. 1d.

With the current set up used, dry CNF + CMC extrusion output rates of up to 0.25 ± 0.072 kg/h and nozzle speeds of up to 7.68 ± 2.22 m/min were possible at a screw speed of 110 rpm. Although the nozzle speeds are lower than those typically reported in conventional spinning processes (20–150 m/min) (Lundahl et al. 2017), filament die extrusion can process larger diameter cord (> 1 mm) versus those typically seen for spinnerets (10–500 mm)(Mather and Wardman 2011), making it a more effective bulk processing methodology. Additionally, larger diameter cord allowed for easier handling and collection as the wet cord extrudate was relatively fragile and does not strain harden as conventional synthetic polymeric filament.

The mechanical properties of the processed CNF + CMC cords are not expected to be higher than those typically observed for CNF, (2,2,6,6-tetramethylpiperidin-1-yl)oxidanyl (TEMPO) oxidized CNF or composite fiber filaments prepared using wet- or dry- spinning methodologies(Håkansson et al. 2014; Kafy et al. 2017; Clarkson et al. 2019). This is due to the lower shear rates typically observed in larger nozzles and the lack of filament drawing, both of which facilitate CNF fibril alignment in the axial direction and improve the mechanical properties. However, the intent of this report is to understand the redispersion and setting behavior of highly loaded CNF + CMC systems rather than improve the mechanical performance of the extruded filament/cord.

The surface morphology of the oven dried and untreated CNF + CMC cords with a varying CMC degree of substitution (D.S. = 0.7, 0.9, and 1.2) is shown in Fig. 2 below. It is evident that there is a lack of fibril

alignment when Fig. 2 is compared to other reported drawn CNF filament micrographs(Kim et al. 2019; Cai et al. 2020). Furthermore, there appears to be no difference between cords prepared with CMC with a D.S. of 0.7 and 0.9 (Fig. 2a and Fig. 2b, respectively), while the cord prepared with a D.S. of 1.2 appeared to have a slightly rougher surface (Fig. 2c).

CMC Adsorption onto CNF fibrils

As mentioned in the introduction, CMC has been reported to adsorb irreversibly to the surface of CNF even under mild heating conditions (22°C) in low solids (~ 1 wt.%) suspensions in water(Butchosa and Zhou 2014). This adsorption occurs due to the attachment of unsubstituted CMC cellulose units onto the surface of exposed cellulose chains on CNF fibrils through hydrogen bonding and can be improved if cations (e.g., Ca^{2+}) are added to the CNF suspension(Duker et al. 2007; Liu et al. 2011). In this work, both the Banbury high-shear mixing process and the relatively high mixing temperatures (55°C) used to prepare CNF + CMC pastes also caused CMC to adsorb irreversibly to the surface of CNF even at high solids loadings (~ 18 wt.%). This was confirmed through zeta potential and titration measurements on dilute CNF + CMC suspensions prepared from the different pastes. As shown in Table 1, CMC adsorption caused an increase in surface charge from − 36.8 ± 2.04 mV for pure CNF to -59.3 ± 1.31 mV for CNF + CMC (D.S. = 0.7). Additionally, there was no statistical difference between the three CMC degrees of substitution with respect to zeta potential (one-way ANOVA: $F_{2,21}$ = 2.22, P = 0.133, R^2 = 0.175). This could mean that the surfaces were completely saturated even with a more negative CMC with a D.S. of 1.2.

As shown in Table 1, titration of the different CNF + CMC suspensions with NaOH revealed the presence of weak acid functionalities from the adsorbed CMC's carboxylic acids. More specifically, surface charge increased from 0.094 ± 0.005 mmol/g COOH for pure CNF to 0.166 ± 0.035 mmol/g COOH for CNF + CMC with a degree of substitution of 0.9. However, while zeta potential revealed a change in magnitude of surface charge (mV) for all D.S. in CNF + CMC when compared to pure CNF, titrated surface charges for CNF + CMC with a D.S. of 0.7 and 1.2 were not significantly different to pure CNF (0.104 ± 0.024 and 0.082 ± 0.012 mmol/g COOH, respectively). As expected, the titrated charges for pure CNF and CNF + CMC are lower than those typically observed for TEMPO oxidized CNF (up to 1.5 mmol/g) (Lasseuguette 2008; Jiang and Hsieh 2016) due to the lower level of carboxylic functionalities.

Table 1
Zeta potential and titration of dilute pure CNF and CNF + CMC suspensions. Each suspension was mixed, centrifuged, and resuspended in water 3 times to remove non-adsorbed CMC or other loose species. Eight measurements per sample were carried out for zeta potential analysis while 3 measurements per sample were performed for titration. The average and standard deviation of the samples are displayed. 5 mM NaOH was used for titration.

Suspension Type	Ave. Zeta Potential [mV] ± STD	Surface Charge [mmol/g COOH] ± STD
Pure CNF	-36.8 ± 2.04	0.094 ± 0.005
CNF + CMC (D.S. = 0.7)	-59.3 ± 1.31	0.104 ± 0.024
CNF + CMC (D.S. = 0.9)	-58.1 ± 2.02	0.166 ± 0.035
CNF + CMC (D.S. = 1.2)	-58.4 ± 2.06	0.082 ± 0.012

Given that CMC adsorption was present, its plausible that the CNF fibril's ability to form irreversible hydrogen bonds between themselves was suppressed. Hence, the pelletized and untreated cord was able to rehydrate itself rapidly (under 20 min) without any stirring/mixing as shown in Fig. 3(a-c). These rehydrated pellets were re-mixed using the same Banbury mixer and reformed into the original ~ 18 wt.% paste as shown in Fig. 3d. Complete re-mixing was confirmed by an equivalent torque reading on the mixer when compared to a freshly prepared CNF + CMC paste (see Figure S8). It is important to note that the torque plateau for the rehydrated CNF + CMC pellets was reached in less than 2 min verses the original ~ 19 min (see Figure S8), hence complete re-mixing was easily and quickly achieved. Furthermore, this paste was re-extruded into a cord without any difficulty and dried as shown in Fig. 3e and Fig. 3f and appeared identical to the original cord before pelletizing (Fig. 1c). Importantly, this shows that by adding CMC, the material can be extruded, dried, pelletized, rehydrated, and extruded to the same consistency to "close the loop", which conceptually allows dry shipment of material.

Dispersibility and Setting Behavior of CNF + CMC

To evaluate the dispersibility and setting behavior of highly loaded CNF + CMC pastes, different chemical treatments were selected and applied to the extruded wet cords. The treatments assessed were HCl, $CaCl_2$, PEI, CDI, PAE, and PAmE. Light scattering techniques like turbidity are often used to monitor the degree of fibrillation/quality during CNF manufacturing processes(Moser et al. 2015; Desmaisons et al. 2017) and, in this work, served to gauge the level of redispersion achieved by the treated and untreated dry CNF + CMC materials in water. Turbidity results in Fig. 4e show that complete redispersion is observed when the dried-untreated CNF + CMC samples (~ 29 NTU) are compared to the never-dried CNF + CMC dilute suspensions (~ 30 NTU), regardless of CMC's degree of substitution. On the other hand, chemical treatment with HCl, CDI, PAE and PAmE all significantly suppressed the level of redispersion achieving a value of less than 1 NTU when compared to the control groups of never-dried pure CNF (~ 29 NTU), never-dried CNF + CMC (~ 30 NTU), and dried-untreated CNF + CMC (~ 29 NTU). As shown in Fig. 4(a-d) and Figure S9, complete redispersion was assessed visually where no observable macroscopic pellets were left in the suspension after mixing versus clearly visible pellets that did not redisperse (i.e., semi-permanent setting). Furthermore, pellets treated with HCl, CDI, PAE, or PAmE did not show any sign of redispersion even after 4 weeks of being immersed in water.

Unlike PAmE, PAE, CDI, and HCl, treatment with PEI and $CaCl_2$ did not seem to suppress the redispersion behavior of CNF + CMC possibly due to the inability of these treatments to form crosslinks between CNF fibrils which then permitted the adsorbed CMC to redisperse them as shown in Figure S9. It is important to note that the lower turbidity values observed for the PEI treatment (~ 19 NTU) are due to the strong cationic nature of the ammonium groups which caused the negatively charged fibrils to flocculate while in suspension rather than the lack of pellet redispersion. This was confirmed through a solids contents measurement of the supernatant (~ 1 wt.%) after redispersion which matched with the original target concentration (1 wt.%) when water was added to the dry pellets. Additionally, for all treatments studied, the degree of carboxymethylation or substitution (D.S. = 0.7, 0.9, and 1.2) of CMC appears to have no significant effect on the level of redispersion.

For the best performing setting treatments (HCl, CDI, PAE, and PAmE) dispersion in a strong alkaline solution (0.1 M NaOH, pH > 10) was also performed. The different treatments were assessed at two curing temperatures. Dispersion in NaOH helped isolate the effect of the different treatments on crosslinking by promoting negative surface charges on CMC by neutralizing any acid present, thus improving the swelling and dispersion behavior of CNF + CMC fibrils(Uetani and Yano 2012). This then revealed differences between treatments which were not evident in water (pH ~ 7). The results in Fig. 5b show that HCl was effective regardless of the curing temperature achieving low turbidity values (6.7 NTU for 25°C and 6.0 NTU for 70°C, respectively) while PAmE and CDI were only effective at their higher curing temperatures of 85°C and 70°C achieving turbidity values of ~ 4 NTU and ~ 3 NTU, respectively. PAE was not effective regardless of the curing temperature hence high turbidity values were observed (23.9 NTU for 25°C and 17.7 NTU for 85°C), however there was a difference between the dispersion behavior observed for a cure temperature of 85°C and 25°C, (one-way ANOVA: $F_{1,10}$ = 74.3, $P = 6.1 * 10^{-6}$, R^2 = 0.881). The difference in dispersion behavior observed between the two different curing temperatures for CDI, PAE and PAmE suggests the formation of physical crosslinks rather than purely structural irreversibly changes that might have occurred during drying (i.e., hornification), while at higher temperatures chemical crosslinking occurs(Fernandes Diniz et al. 2004). As shown in Figure S10 and Fig. 5a small pellet fragments were visible for all treatments hence some level of dispersion was still possible in the studied time period (24 h).

Optical micrographs, shown in Fig. 6, of the redispersed CNF + CMC fibrils in water and 0.1 M NaOH revealed that the fibril's morphology remained intact before and after redispersion when compared to never-dried pure CNF (Fig. 6a) and dried-untreated CNF + CMC (Fig. 6b). It is important to note that the reduced presence of CNF fibrils displayed in the micrographs for CDI (Fig. 6c), HCl (Fig. 6d), PAE (Fig. 6e), and PAmE (Fig. 6f) match with the results obtained for turbidity. Perhaps only non-crosslinked and or smaller fibrils were able to be redispersed back into the solution. Furthermore, expanded optical micrographs show the same behavior (see Figure S11 and Figure S12).

FTIR Analysis of Treated CNF + CMC

To understand the possible setting mechanism behind the chemical treatments (HCl, CDI, PAE, and PAmE) which significantly suppressed the dispersibility of CNF + CMC, FTIR was used. As shown in Figure S13 through Figure S16, complete spectra (550 cm^{-1} to 4000 cm^{-1}) were captured for each treatment at two curing temperatures. As expected for all samples, common cellulose IR peaks at 3335 cm^{-1}, 2899 cm^{-1}, 1429 cm^{-1}, 1368 cm^{-1}, 1335 cm^{-1}, 1024 cm^{-1}, and 896 cm^{-1} were observed. These peaks were assigned to the O-H hydroxyl stretching, C-H stretching, and bending and stretching of -CH_2, -CH, -OH, and C-O bonds in cellulose, respectively(Aguayo et al. 2018; Hospodarova et al. 2018).

Further analysis of the 1000 cm^{-1} to 1800 cm^{-1} spectrum region, shown in Fig. 7, revealed key peak differences between the treated CNF + CMC samples and the control groups of pure CMC powder, pure CNF, untreated CNF + CMC, and cured pure compounds of CDI, PAE, and PAmE. As shown in Fig. 7a treatment with HCl caused the formation of a strong peak at 1731 cm^{-1} which was assigned to the carbonyl stretching of newly formed ester linkages (i.e., COOC) or, equally likely, the carbonyl stretching of protonated carboxylates (i.e., COOH)(Müller et al. 2010). This occurred for both curing temperatures (25°C and 70°C). The peak at 1591 cm^{-1} which was observed only for CMC powder and untreated CNF + CMC was assigned to the asymmetric stretching vibration of the carboxylate (COO^-) moiety(Cuba-Chiem et al. 2008; Eyholzer et al. 2010; Onyianta et al. 2018). It is important to note that the peak at 1591 cm^{-1} was not present for HCl 25°C or HCl 70°C, indicating a possible replacement of COO^- groups with ester linkages or, due to the high acidity of 0.1 M HCl treatment, the protonation of the carboxylate that caused a shift of the 1591 cm^{-1} peak to 1731 cm^{-1} as shown by Cuba-Chiem et. al(Cuba-Chiem et al. 2008). Protonation and esterification could not be separated due to the similarity of the peak locations for the C = O stretching vibration which typically lies between 1760 – 1700 cm^{-1}. However, esterification crosslinking between CNF fibrils with adsorbed CMC could possibly explain the suppressed dispersibility behavior observed for both cure temperatures during turbidity measurements (Fig. 5b). A schematic of the possible ester linkages between CNF fibrils with adsorbed CMC is shown in Fig. 8a(Pantze et al. 2008; Müller et al. 2010). The weak peak observed at 1645 cm^{-1} was assigned to the (O-H) bending vibration of adsorbed/bound water on CNF fibrils which was present in all samples CNF + CMC samples and pure CNF(Eyholzer et al. 2010; Rosa et al. 2010; Carrillo et al. 2018).

As shown in Fig. 7b, treatment with CDI lead to prominent absorption peaks located at 1754 cm^{-1}, 1716 cm^{-1}, 1639 cm^{-1}, 1549 cm^{-1}, 1448 cm^{-1}, 1247 cm^{-1}, and 1033 cm^{-1}. The appearance of these peaks could be understood through two possible reaction pathways between carbodiimides and CMC's protonated carboxylates, both of which start with the formation of unstable O-acyl urea as a reaction intermediate. The first reaction route leads to the formation of stable N-acyl urea linkages formed from the rearrangement of O-acyl urea(Hesselmans et al. 2006; Posthumus et al. 2007). The formation of new N-acyl urea linkages between the adsorbed CMC repeat units can then possibly explain the observed 1639 cm^{-1} (C = O stretching, CONH) and 1549 cm^{-1} peak (N-H bending)(Posthumus et al. 2007; Derksen 2017). However, because these peaks were also present in the spectra for pure CDI cured at 70°C (shown by the dotted vertical lines in Fig. 7b), they could simply originate from the added presence of the resin in

the CNF + CMC system. The second CDI-carboxylic acid reaction route leads to the formation of anhydride linkages and urea as byproduct from the reaction between O-acyl urea and a additionally available carboxylic acid(Posthumus et al. 2007). The formation of anhydride linkages can then possibly explain the observed strong 1033 cm^{-1} peak (CO-O-CO stretching) and the 1754 cm^{-1} peak (C = O stretching), which were not present in the pure CDI spectra (shown by the dashed lines in Fig. 7b), while the 1448 cm^{-1} (N-C-N asymmetric stretching) and the 1247 cm^{-1} peak (C-N stretching, amine) can be linked to the urea byproduct(Piasek Z. and Urbanski T. 1962; Lu et al. 2016). A schematic of the possible anhydride linkages formed between CNF fibrils with adsorbed CMC is shown in Fig. 8b(Posthumus et al. 2007).

There is also the possibility that ester linkages were formed between CMC units through a subsequent reaction between anhydride linkages and a nucleophile like that of a hydroxyl from either CMC or CNF leading to intra- or inter-molecular linkages which could also explain the appearance of the 1754 cm^{-1} peak/shoulder (C = O stretching, COOC) which was not present for the pure CDI compound (see dashed line in Fig. 7b)(Posthumus et al. 2007; Mojarradi 2011). The peak observed at 1716 cm^{-1} (C = O stretching) could belong to carboxylic acids which were not converted during the CDI reaction. It is important to note that both reaction routes can occur simultaneously and the ratio between N-acyl urea and anhydride/urea has been reported to be dependent on the mobility of the reactive groups and ratio of concentration between carbodiimide and carboxyl groups(Posthumus et al. 2007). Additionally, similar to treatment with HCl, the lack of the 1592 cm^{-1} peak for either CDI 25°C and CDI 70°C points to a possible consumption of the (COO^-) groups for the formation of N-acyl urea, anhydride, and ester linkages as well as the possible protonation of the carboxylates due to the low pH at treatment (0.1 M HCl). Although both CDI 25°C and CDI 70°C appeared to contain the same major peaks in the 1000 cm^{-1} to 1800 cm^{-1} region, the disappearance of the 2117 cm^{-1} peak (assigned to the -N = C = N- stretching vibration of carbodiimides(Pham and Winnik 2006)) shown in Figure S17, confirmed that a higher curing temperature (70°C) was necessary for complete CDI resin reaction/activation. Hence, the lack of complete CDI activation could possibly explain the much higher turbidity values observed for the CDI treatment cured at 25°C (27.6 NTU) when compared to the CDI treatment cured at 70°C (3.3 NTU) as shown in Fig. 5b.

Treatment with PAE, shown in Fig. 7c, revealed amide I and amide II peaks at 1641 cm^{-1} (C = O stretching, CONH) and 1546 cm^{-1} (N-H bending), respectively. These were also present in the spectra for pure PAE cured at 85°C (see vertical dotted lines in Fig. 7c and Fig. 8c for the backbone structure) and are likely due to the added presence of the resin in the CNF + CMC system rather than the formation of new amide linkages between CMC units. However, carbonyl stretching vibrations of ester linkages (COOC) were observed at two different adsorption bands, one for PAE treated CNF + CMC (1742 cm^{-1}, dashed line) and one for pure PAE cured at 85°C (1732 cm^{-1}, dotted line). For PAE treated CNF + CMC, esterification has been reported to be the primary crosslinking mechanism behind the wet strength development or improvement in other (COO^-) containing nanocellulose systems like that of TEMPO oxidized CNF and cellulose ethers like CMC(Obokata and Isogai 2007; Siqueira et al. 2015; Sharma and Deng 2016; Yang et

al. 2017). The ester bonds are formed from the thermally induced reaction between (COO^-) and the azetidinium groups in the PAE resin(Siqueira et al. 2015). A schematic of the possible ester linkages between CNF fibrils with adsorbed CMC is shown in Fig. 8c(Yang et al. 2018). On the other hand, pure PAE has been reported to crosslink with itself forming ester linkages though its tail end carboxylates or, as a secondary crosslinking reaction, form 2-propanol linkages between the azetidinium groups on its backbone(Obokata and Isogai 2007; Chattopadhyay et al. 2013; Siqueira 2014). Hence, PAE esterification with CMC and self-crosslinking could possibly explain the shift or appearance of the two ester absorption bands as shown in Fig. 7c. It is important to note that while HCl and CDI treatment may have led to protonation of CMC's carboxylate groups, treatment with PAE or PAmE did not require a low pH and hence the peaks observed are likely ester carbonyl stretching vibrations. When the two cure temperatures (25°C and 85°C) are compared, the ester band (1742 cm^{-1}) is almost not present for the 25°C cured sample possibly due to a reduced number of linkages formed, hence it was much easier for CNF + CMC to redisperse as seen in the higher turbidity values (see Fig. 5b, 23.9 NTU for 25°C verses 17.7 NTU for 85°C).

As shown in Fig. 7d, a similar spectrum to the PAE treatment was observed for treatment with PAmE. Again, the amide peaks simply confirmed the presence of the PAmE resin in the CNF + CMC system as these were also present in the pure PAmE cured at 85°C spectra (dotted lines). Similar to PAE, two different absorptions bands for carbonyl stretching of esters were observed, one at 1742 cm^{-1} (dashed line) for PAmE treated CNF + CMC and one at 1732 cm^{-1} (dotted line) for pure PAmE cured at 85°C. This is possibly due to the fact that both resin systems (PAE and PAmE) can react with the same functional groups (carboxylates, hydroxyls, thiols, and amines) which led to identical crosslinking linkages. Perhaps the only difference between the two resin spectra (PAE verses PAmE) is the lower peak intensities observed for PAmE. However, the performance of PAmE was superior in terms of redispersion suppression to that of PAE, as observed in Fig. 5b. The reason for this is unknown but could be linked to the high cationic charge of PAmE which might have allowed for the resin to interact more strongly with the exposed (COO^-) groups in CMC or other slightly negative charges on the surface of CNF fibrils as well as go into the nanopores between fibrils(Yang et al. 2017). Furthermore, it is important to note that unlike all other treatments, the carboxylate peak (1592 cm^{-1}) was not consumed significantly for either cure temperature (25°C and 85°C). When the two cure temperatures are compared for treatment with PAmE, the intensity for the 1732 cm^{-1} peak for a cure temperature of 25°C were of weaker intensity when compared to the spectra for 85°C, which might explain the much higher turbidity value of 21.7 NTU when compared to 3.9 NTU, respectively (see Fig. 5b).

Table 2

Peak intensity normalized by the invariant peak intensity at 1024 cm^{-1}.

Treatment type and cure temperature (°C)	1033/1024 (CO-O-CO stretch, anhydride)	1549/1024 (Amide II, N-H bend, CONH)	1591/1024 (COO^- asymmetric stretch)	1641/1024 (Amide I, C = O stretch, CONH or H-O stretch)	1731/1024 (C = O stretch, COOC or COOH)	1754/1024 (C = O stretch, COOC or CO-O-CO)
HCl 70°C	0.996	0.045	0.058	0.118	0.186	0.138
HCl 25°C	0.988	0.066	0.080	0.133	0.188	0.147
CDI 70°C	1.082	0.336	0.112	0.278	0.203	0.124
CDI 25°C	1.018	0.109	0.071	0.141	0.113	0.084
PAE 85°C	1.024	0.323	0.226	0.413	0.112	0.100
PAE 25°C	1.018	0.245	0.194	0.316	0.073	0.064
PAmE 85°C	1.021	0.087	0.151	0.139	0.076	0.074
PAmE 25°C	1.018	0.095	0.167	0.153	0.065	0.061
Pure CNF	1.003	0.027	0.036	0.056	0.027	0.026
Pure CMC	0.996	0.338	0.877	0.299	0.081	0.084
Untreated CNF + CMC	0.982	0.079	0.182	0.129	0.057	0.054

Table 2 summarizes the FTIR results shown in Fig. 7 where the intensity of the main peaks of interest (1033 cm^{-1}, 1549 cm^{-1}, 1591 cm^{-1}, 1641 cm^{-1}, 1731 cm^{-1}, and 1754 cm^{-1}) was normalized by that of the intensity of the invariant 1024 cm^{-1} peak assigned to the C-O stretching in cellulose(Colom et al. 2003; Lionetto et al. 2012). Overall, due to the numerous different reaction routes, treatment with CDI could have led to the formation of ester, N-acyl urea, anhydride, or all of the above linkages which made it a very effective treatment for the setting of CNF + CMC. PAmE was an equally effective setting treatment possibly due to the formation of ester linkages and, unlike PAE, had a high cationic charge which might have improved its interaction with CMC's carboxylate groups. However, both of these treatments were only effective when cured at higher temperatures (70°C and 85°C, respectively). On the other hand, HCl was effective even when cured at room temperature (25°C). Lastly, PAE was the least effective setting treatment for CNF + CMC regardless of the curing temperature.

Water Uptake of Treated CNF + CMC

Water uptake of the differently treated CNF + CMC with a D.S. of 0.7 agreed with both the observed turbidity behavior and the possibly newly formed linkages detected through FTIR. For example, the best performing setting treatments of HCl and CDI (both cured at 70°C) absorbed on average only 20.1 ± 0.19 %, and 17.5 + 0.58 % of their weight in water, respectively. PAE and PAmE treated CNF + CMC (both cured

at 85°C) absorbed 41.6 ± 0.32 % and 59.7 ± 1.1 % of their weight in water, respectively. The higher water uptake for the PAE and PAmE treated CNF + CMC led to a much more flexible structure which could, in turn, be more susceptible to redispersion by mechanical stirring (i.e., softer structure). On the other hand, HCl and CDI treated materials were much more rigid and possibly less susceptible to redispersion by stirring. The flexibility of the treated CNF + CMC materials is qualitatively shown in Figure S18. Unlike HCl and CDI, hydrated PAE and PAmE treated CNF + CMC cord segments could be folded onto itself without fracturing into two pieces.

Ramifications of efforts

More broadly, the results obtained show that the redispersion and setting behavior of CNF with adsorbed CMC can be controlled through different chemical treatments. Industrially, redispersion grants the ability to transport CNF in a dry state, thus providing a significant reduction in weight and transportation cost. On the other hand, semi-permanent setting of CNF + CMC systems allows for CNF products (e.g., sheets, cups, lids, clamshells, etc.) to retain their shape after being processed while at the same time reducing their susceptibility to high humidity conditions, and hence extending the life of use and expanding their possible applications. Furthermore, bulk processing of CNF + CMC through conventional polymer processing equipment like a Banbury high-shear mixer, a single-screw extruder, and a commercial pelletizer takes advantage of the already developed polymer melt-processing industry and reduces the initial capital investment destined for new processing equipment.

Conclusion

Highly loaded CNF+CMC pastes (~18 wt.%) were prepared and continuously processed into cord using a single-screw extruder. Output rates of up to 0.25 ± 0.072 kg/h (dry) and nozzle speeds of up to 7.68 ± 2.22 m/min were possible with the current set up. Thus, proving to be a successful bulk processing technique for highly loaded CNF+CMC systems. Zeta potential of never dried and dilute CNF+CMC suspensions showed a change in surface charge from -36.8 mV for pure CNF to -59.3 mV for CNF+CMC (D.S. = 0.7). Titration of the CNF+CMC suspensions with NaOH revealed the presence of weak acid functionalities attributed to the adsorbed CMC's carboxylic acids and showed an increase in surface concentration from 0.094 ± 0.005 mmol/g COOH for pure CNF to 0.166 ± 0.035 mmol/g COOH for CNF+CMC (D.S. = 0.9). Due to the adsorbed CMC on the CNF fibrils, dried-untreated CNF+CMC could be completely redispersed in water at room temperature conditions and allowed for complete remixing and re-extrusion back into a cord. Turbidity measurements confirmed that dried-untreated CNF+CMC fully redispersed, reaching values of ~29 NTU when compared to never-dried CNF+CMC (~30 NTU). On the other hand, chemical treatment with HCl, CDI, PAE, and PAmE almost entirely suppressed the dispersibility of dried-untreated CNF+CMC achieving turbidity values of less than 1 NTU. Overall, the dispersibility observed for dried untreated and treated CNF+CMC was not dependent on the degree of substitution of CMC. Subsequently, dispersion in a strongly alkaline solution (0.1 M NaOH) showed that HCl treatment was effective regardless of the curing temperature achieving low turbidity values (6.7 NTU for 25 °C and 6.0 NTU for 70 °C) while CDI and PAmE treatments were effective only at the higher curing temperatures

(85 °C and 70 °C) achieving turbidity values of ~3 NTU and ~4 NTU, respectively. Treatment with PAE was the least effective, hence relatively high turbidity values were observed (23.9 NTU for 25 °C and 17.7 NTU for 85 °C) when compared to the other chemical treatments at either cure temperatures. Depending on the chemical treatment used, FTIR analysis of the treated CNF+CMC samples revealed the presence of possible ester, N-acyl urea, and anhydride linkages which could possibly explain the suppressed redispersion behavior. Lastly, water uptake of the differently treated and dried CNF+CMC materials agreed with both turbidity and FTIR results.

Declarations

Funding: The authors would like to acknowledge the financial support provided by the US Endowment and the Public-Private Partnership for Nanotechnology (Grant Number: 109217)

Conflicts of interest/Competing interests: The authors have no conflicts of interest to declare.

Availability of data and material: Additional information regarding this manuscript can be found free of charge in the supporting information.

Code availability: Not applicable.

Authors' contributions: All authors contributed to the study conception and design. Material preparation, data collection and analysis were performed by Sami M. El Awad Azrak and Jared A. Gohl. The first draft of the manuscript was written by Sami M. El Awad Azrak and all authors commented on previous versions of the manuscript. All authors read and approved the final manuscript.

Ethics approval: All authors have read and understood the "Ethical Responsibilities of Authors" in the journal's "Submission Guidelines", including the passage on screening for plagiarism with computer software.

Consent to participate: Not applicable.

Consent for publication: All authors have fully read, agreed, and approved the final version of the manuscript which has been submitted for possible publication.

Supporting Information

The following information is provided free of charge:

- TEM images of CNF fibrils at two different magnifications (PDF)
- Video recording of the extrusion and collection process for CNF+CMC pastes (mp4)
- Video recording of the pelletization of dry CNF+CMC cord (mp4)
- Photograph of wet and dry CNF+CMC cord segments (PDF)

- Representative titration curves (PDF)
- Photograph of CNF+CMC cord treated with HCl and cured at different temperatures (PDF)
- Analysis of the penetration rate of HCl into CNF+CMC (PDF)
- Plastogram/torque curves for the mixing of rehydrated CNF+CMC pellets and a freshly prepared CNF+CMC paste (PDF)
- Photograph of redispersed CNF+CMC pellets after stirring in DI water and NaOH (PDF)
- Optical micrographs of redispersed CNF fibrils (PDF)
- FTIR spectra of HCl, CDI, PAE, and PAmE treated CNF+CMC (PDF)

References

Aguayo MG, Pérez AF, Reyes G, et al (2018) Isolation and characterization of cellulose nanocrystals from rejected fibers originated in the Kraft Pulping process. Polymers (Basel) 10:. https://doi.org/10.3390/polym10101145

Assis CA de, Iglesias MC, Bilodeau M, et al (2018) Cellulose micro- and nanofibrils (CMNF) manufacturing - financial and risk assessment. Biofuels, Bioprod Biorefining 12:251–264. https://doi.org/10.1002/bbb.1835

Axelsson L, Franzén M, Ostwald M, et al (2012) Perspective: Jatropha cultivation in southern India: Assessing farmers' experiences. Biofuels, Bioprod Biorefining 6:246–256. https://doi.org/10.1002/bbb

Beghello L, Lindström T (1998) The influence of carboxymethylation on the fiber flocculation process. Nord Pulp Pap Res J 13:269–273

Butchosa N, Zhou Q (2014) Water redispersible cellulose nanofibrils adsorbed with carboxymethyl cellulose. Cellulose 21:4349–4358. https://doi.org/10.1007/s10570-014-0452-7

Cai Y, Geng L, Chen S, et al (2020) Hierarchical Assembly of Nanocellulose into Filaments by Flow-Assisted Alignment and Interfacial Complexation: Conquering the Conflicts between Strength and Toughness. ACS Appl Mater Interfaces 12:32090–32098. https://doi.org/10.1021/acsami.0c04504

Carrillo I, Mendonça RT, Ago M, Rojas OJ (2018) Comparative study of cellulosic components isolated from different Eucalyptus species. Cellulose 25:1011–1029. https://doi.org/10.1007/s10570-018-1653-2

Chattopadhyay S, Keul H, Moeller M (2013) Synthesis of azetidinium-functionalized polymers using a piperazine based coupler. Macromolecules 46:638–646. https://doi.org/10.1021/ma302008s

Clarkson CM, El Awad Azrak SM, Chowdhury R, et al (2019) Melt Spinning of Cellulose Nanofibril/Polylactic Acid (CNF/PLA) Composite Fibers For High Stiffness. ACS Appl Polym Mater 1:160–168. https://doi.org/10.1021/acsapm.8b00030

Clarkson CM, El Awad Azrak SM, Forti ES, et al (2020a) Recent Developments in Cellulose Nanomaterial Composites. Adv. Mater.

Clarkson CM, El Awad Azrak SM, Schueneman GT, et al (2020b) Crystallization kinetics and morphology of small concentrations of cellulose nanofibrils (CNFs) and cellulose nanocrystals (CNCs) melt-compounded into poly(lactic acid) (PLA) with plasticizer. Polymer (Guildf) 187:122101. https://doi.org/10.1016/j.polymer.2019.122101

Colom X, Carrillo F, Nogués F, Garriga P (2003) Structural analysis of photodegraded wood by means of FTIR spectroscopy. Polym Degrad Stab 80:543–549. https://doi.org/10.1016/S0141-3910(03)00051-X

Cuba-Chiem LT, Huynh L, Ralston J, Beattie DA (2008) In situ particle film ATR FTIR spectroscopy of carboxymethyl cellulose adsorption on talc: Binding mechanism, pH effects, and adsorption kinetics. Langmuir 24:8036–8044. https://doi.org/10.1021/la800490t

Derksen AJ (2017) Polycarbodiimides as classification-free and easy to use crosslinkers for water-based coatings. Waalwijk, The Netherlands

Desmaisons J, Boutonnet E, Rueff M, et al (2017) A new quality index for benchmarking of different cellulose nanofibrils. Carbohydr Polym 174:318–329. https://doi.org/10.1016/j.carbpol.2017.06.032

Duker E, Brännvall E, Lindström T (2007) The effects of CMC attachment onto industrial and laboratory-cooked pulps. Nord Pulp Pap Res J 22:356–363. https://doi.org/10.3183/npprj-2007-22-03-p356-363

El Awad Azrak SM, Clarkson CM, Moon RJ, et al (2019) Wet-Stacking Lamination of Multilayer Mechanically Fibrillated Cellulose Nanofibril (CNF) Sheets with Increased Mechanical Performance for Use in High-Strength and Lightweight Structural and Packaging Applications. ACS Appl Polym Mater 1:2525–2534. https://doi.org/10.1021/acsapm.9b00635

El Awad Azrak SM, Costakis WJ, Moon RJ, et al (2020) Continuous Processing of Cellulose Nanofibril Sheets Through Conventional Single-Screw Extrusion. ACS Appl Polym Mater 2:3365–3377. https://doi.org/10.1021/acsapm.0c00477

Eyholzer C, Bordeanu N, Lopez-Suevos F, et al (2010) Preparation and characterization of water-redispersible nanofibrillated cellulose in powder form. Cellulose 17:19–30. https://doi.org/10.1007/s10570-009-9372-3

Feddersen RL, Thorp SN (2012) Sodium Carboxymethylcellulose. In: Industrial Gums: Polysaccharides and Their Derivatives: Third Edition, Third Edit. ACADEMIC PRESS, INC., pp 537–578

Fernandes Diniz JMB, Gil MH, Castro JAAM (2004) Hornification - Its origin and interpretation in wood pulps. Wood Sci Technol 37:489–494. https://doi.org/10.1007/s00226-003-0216-2

Foster EJ, Moon RJ, Agarwal UP, et al (2018) Current characterization methods for cellulose nanomaterials. Chem Soc Rev 47:2609–2679. https://doi.org/10.1039/c6cs00895j

Håkansson KMO, Fall AB, Lundell F, et al (2014) Hydrodynamic alignment and assembly of nanofibrils resulting in strong cellulose filaments. Nat Commun 5:. https://doi.org/10.1038/ncomms5018

Hesselmans LCJ, Derksen AJ, Van Den Goorbergh JAM (2006) Polycarbodiimide crosslinkers. Prog Org Coatings 55:142–148. https://doi.org/10.1016/j.porgcoat.2005.08.011

Hospodarova V, Singovszka E, Stevulova N (2018) Characterization of Cellulosic Fibers by FTIR Spectroscopy for Their Further Implementation to Building Materials. Am J Anal Chem 09:303–310. https://doi.org/10.4236/ajac.2018.96023

Jiang F, Hsieh Y Lo (2016) Self-assembling of TEMPO Oxidized Cellulose Nanofibrils As Affected by Protonation of Surface Carboxyls and Drying Methods. ACS Sustain Chem Eng 4:1041–1049. https://doi.org/10.1021/acssuschemeng.5b01123

Kafy A, Kim HC, Zhai L, et al (2017) Cellulose long fibers fabricated from cellulose nanofibers and its strong and tough characteristics. Sci Rep 7:1–8. https://doi.org/10.1038/s41598-017-17713-3

Kaur G, Uisan K, Ong KL, Ki Lin CS (2018) Recent Trends in Green and Sustainable Chemistry & Waste Valorisation: Rethinking Plastics in a circular economy. Curr Opin Green Sustain Chem 9:30–39. https://doi.org/10.1016/j.cogsc.2017.11.003

Kim HC, Kim D, Lee JY, et al (2019) Effect of Wet Spinning and Stretching to Enhance Mechanical Properties of Cellulose Nanofiber Filament. Int J Precis Eng Manuf - Green Technol 6:567–575. https://doi.org/10.1007/s40684-019-00070-z

Lasseuguette E (2008) Grafting onto microfibrils of native cellulose. Cellulose 15:571–580. https://doi.org/10.1007/s10570-008-9200-1

Liimatainen H, Haavisto S, Haapala A, Niinimäki J (2009) Influence of adsorbed and dissolved carboxymethyl cellulose on fibre suspension dispersing, dewaterability, and fines retention. BioResources 4:321–340. https://doi.org/10.15376/biores.4.1.321-340

Lin X, Li Y, Chen Z, et al (2013) Synthesis, characterization and electrospinning of new thermoplastic carboxymethyl cellulose (TCMC). Chem Eng J 215–216:709–720. https://doi.org/10.1016/j.cej.2012.10.089

Lionetto F, Del Sole R, Cannoletta D, et al (2012) Monitoring wood degradation during weathering by cellulose crystallinity. Materials (Basel) 5:1910–1922. https://doi.org/10.3390/ma5101910

Liu Z, Choi H, Gatenholm P, Esker AR (2011) Quartz crystal microbalance with dissipation monitoring and oxymethyl cellulose adsorption onto regenerated cellulose

surfaces. Langmuir 27:8718–8728. https://doi.org/10.1021/la200628a

Lu P, Zhang Y, Jia C, et al (2016) Use of polyurea from urea for coating of urea granules. Springerplus 5:. https://doi.org/10.1186/s40064-016-2120-x

Lundahl MJ, Klar V, Wang L, et al (2017) Spinning of cellulose nanofibrils into filaments: A review. Ind Eng Chem Res 56:8–19. https://doi.org/10.1021/acs.iecr.6b04010

Mather RR, Wardman RH (2011) The Chemistry of Textile Fibres. Royal Society of Chemistry

Mojarradi H (2011) Coupling of substances containing a primary amine to hyaluronan via carbodiimide-mediated amidation. Uppsala University

Moon RJ, Martini A, Nairn J, et al (2011) Cellulose nanomaterials review: structure, properties and nanocomposites. Chem Soc Rev 40:3941–3994. https://doi.org/10.1039/c0cs00108b

Moon RJ, Schueneman GT, Simonsen J (2016) Overview of Cellulose Nanomaterials, Their Capabilities and Applications. JOM 68:2383–2394. https://doi.org/10.1007/s11837-016-2018-7

Moser C, Lindström ME, Henriksson G (2015) Toward industrially feasible methods for following the process of manufacturing cellulose nanofibers. BioResources 10:2360–2375. https://doi.org/10.15376/biores.10.2.2360-2375

Müller Y, Tot I, Potthast A, et al (2010) The impact of esterification reactions on physical properties of cellulose thin films. Soft Matter 6:3680–3684. https://doi.org/10.1039/c0sm00005a

Murray JCF (2009) Cellulosics. In: Handbook of Hydrocolloids: Second Edition. pp 710–723

Obokata T, Isogai A (2007) The mechanism of wet-strength development of cellulose sheets prepared with polyamideamine-epichlorohydrin (PAE) resin. Colloids Surfaces A Physicochem Eng Asp 302:525–531. https://doi.org/10.1016/j.colsurfa.2007.03.025

Onyianta AJ, Dorris M, Williams RL (2018) Aqueous morpholine pre-treatment in cellulose nanofibril (CNF) production: comparison with carboxymethylation and TEMPO oxidisation pre-treatment methods. Cellulose 25:1047–1064. https://doi.org/10.1007/s10570-017-1631-0

Pantze A, Karlsson O, Westermark U (2008) Esterification of carboxylic acids on cellulosic material: Solid state reactions. Holzforschung 62:136–141. https://doi.org/10.1515/HF.2008.027

Pham HH, Winnik MA (2006) Polymer interdiffusion vs cross-linking in carboxylic acid-carbodiimide latex films. Effect of annealing temperature, reactive group concentration, and carbodiimide substituent. Macromolecules 39:1425–1435. https://doi.org/10.1021/ma051685w

Piasek Z., Urbanski T. (1962) The Infrared Absorption Spectrum and Structure of Urea. Bul L' Acad Pol Des

Posthumus W, Derksen AJ, van den Goorbergh JAM, Hesselmans LCJ (2007) Crosslinking by polycarbodiimides. Prog Org Coatings 58:231–236. https://doi.org/10.1016/j.porgcoat.2006.09.031

Rol F, Vergnes B, El Kissi N, Bras J (2020) Nanocellulose Production by Twin-Screw Extrusion: Simulation of the Screw Profile to Increase the Productivity. ACS Sustain Chem Eng 8:50–59. https://doi.org/10.1021/acssuschemeng.9b01913

Rosa MF, Medeiros ES, Malmonge JA, et al (2010) Cellulose nanowhiskers from coconut husk fibers: Effect of preparation conditions on their thermal and morphological behavior. Carbohydr Polym 81:83–92. https://doi.org/10.1016/j.carbpol.2010.01.059

Samaniuk JR, Scott CT, Root TW, Klingenberg DJ (2012) Rheological modification of corn stover biomass at high solids concentrations. J Rheol (N Y N Y) 56:649–665. https://doi.org/10.1122/1.3702101

Samaniuk JR, Scott CT, Root TW, Klingenberg DJ (2015) Effects of process variables on the yield stress of rheologically modified biomass. Rheol Acta 54:941–949. https://doi.org/10.1007/s00397-015-0884-5

Schmid CF, Klingenberg DJ (2000) Properties of Fiber Flocs with Frictional and Attractive Interfiber Forces. J Colloid Interface Sci 226:136–144. https://doi.org/10.1006/jcis.2000.6803

Sehaqui H, Liu A, Zhou Q, Berglund LA (2010) Fast preparation procedure for large, flat cellulose and cellulose/inorganic nanopaper structures. Biomacromolecules 11:2195–2198. https://doi.org/10.1021/bm100490s

Sharma S, Deng Y (2016) Dual mechanism of dry strength improvement of cellulose nanofibril films by polyamide-epichlorohydrin resin cross-linking. Ind Eng Chem Res 55:11467–11474. https://doi.org/10.1021/acs.iecr.6b02910

Shogren R, Wood D, Orts W, Glenn G (2019) Plant-based materials and transitioning to a circular economy. Sustain Prod Consum 19:194–215. https://doi.org/10.1016/j.spc.2019.04.007

Siqueira EJ (2014) Polyamideamine Epichlorohydrin-Based Papers: Mechanisms of Wet Strength Development and Paper Repulping. Universite de Grenoble

Siqueira EJ, Salon M-CB, Belgacem MN, Mauret E (2015) Carboxymethylcellulose (CMC) as a model compound of cellulose fibers and polyamideamine epichlorohydrin (PAE)-CMC interactions as a model of PAE-fibers interactions of PAE-based wet strength papers. J Appl Polym Sci 132:n/a-n/a. https://doi.org/10.1002/app.42144

Uetani K, Yano H (2012) Zeta potential time dependence reveals the swelling dynamics of wood cellulose nanofibrils. Langmuir 28:818–827. https://doi.org/10.1021/la203404g

Watanabe M, Gondo T, Kitao O (2004) Advanced wet-end system with carboxymethyl-cellulose. Tappi

Williams PA, Phillips GO (2009) Introduction to food hydrocolloids. In: Handbook of Hydrocolloids: Second Edition. Woodhead Publishing Limited, pp 1–22

Yan H, Lindström T, Christiernin M (2006) Some ways to decrease fibre suspension flocculation and improve sheet formation. Nord Pulp Pap Res J 21:36–43

Yang D, Diflavio JL, Gustafsson E, Pelton R (2018) Wet-peel: A tool for comparing wet-strength resins. Nord Pulp Pap Res J 33:632–646. https://doi.org/10.1515/npprj-2018-0013

Yang W, Bian H, Jiao L, et al (2017) High wet-strength, thermally stable and transparent TEMPO-oxidized cellulose nanofibril film: Via cross-linking with poly-amide epichlorohydrin resin. RSC Adv 7:31567–31573. https://doi.org/10.1039/c7ra05009g

Zhang Y, Nypelö T, Salas C, et al (2013) Cellulose nanofibrils: From strong materials to bioactive surfaces. J Renew Mater 1:195–211. https://doi.org/10.7569/JRM.2013.634115

Figures

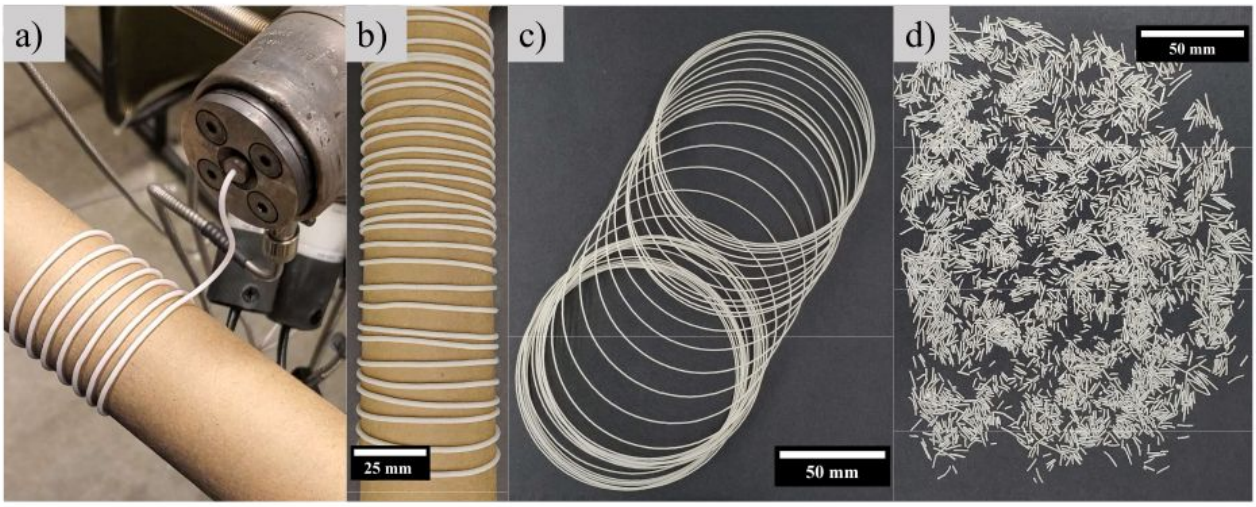

Figure 1

Single-screw filament/cord extrusion of a CNF+CMC paste (at ~18 wt.%) through a 2 mm nozzle (a), collected CNF+CMC wet cord extrudate on a cardboard roll (b), oven dried CNF+CMC cord (c), and pelletized cord (d).

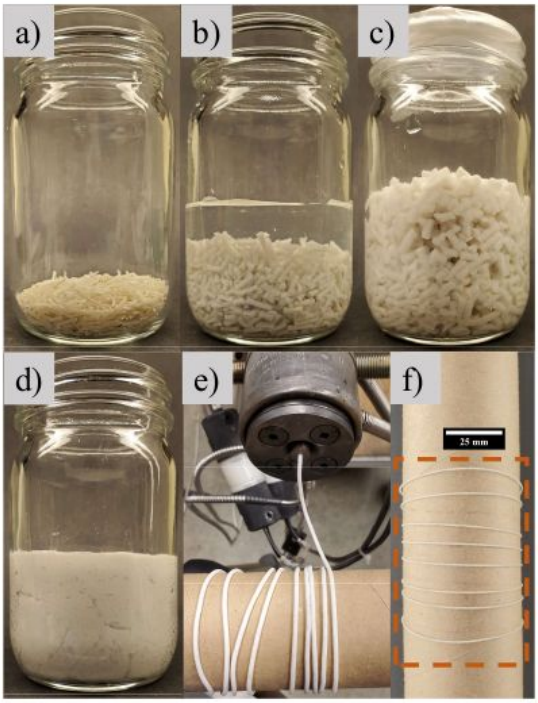

Figure 2

Surface morphology of the extruded and dried untreated CNF+CMC cords with a varying degree of CMC carboxymethylation or substitution of 0.7 (a), 0.9 (b), and 1.2 (c).

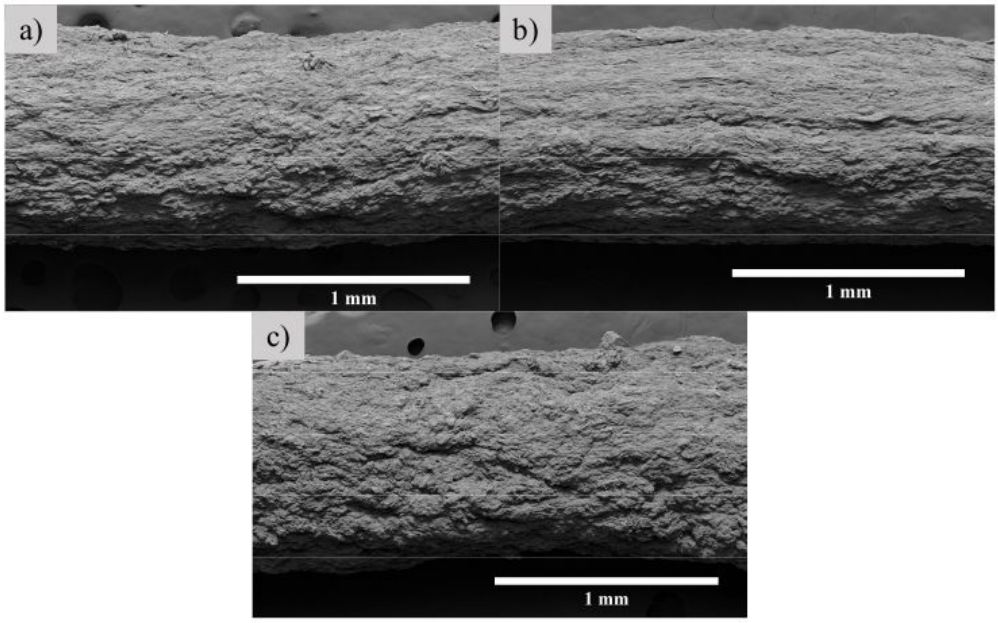

Figure 3

Pelletized untreated CNF+CMC pellets at different stages of the rehydration process starting completely dry (a), ~30 s after adding water (b), 20 min after adding water (c), after being re-mixed in the Banbury shear mixer (d), and re-extruded into a filament/cord (e) and oven dried at 35 °C on a cardboard roll (f).

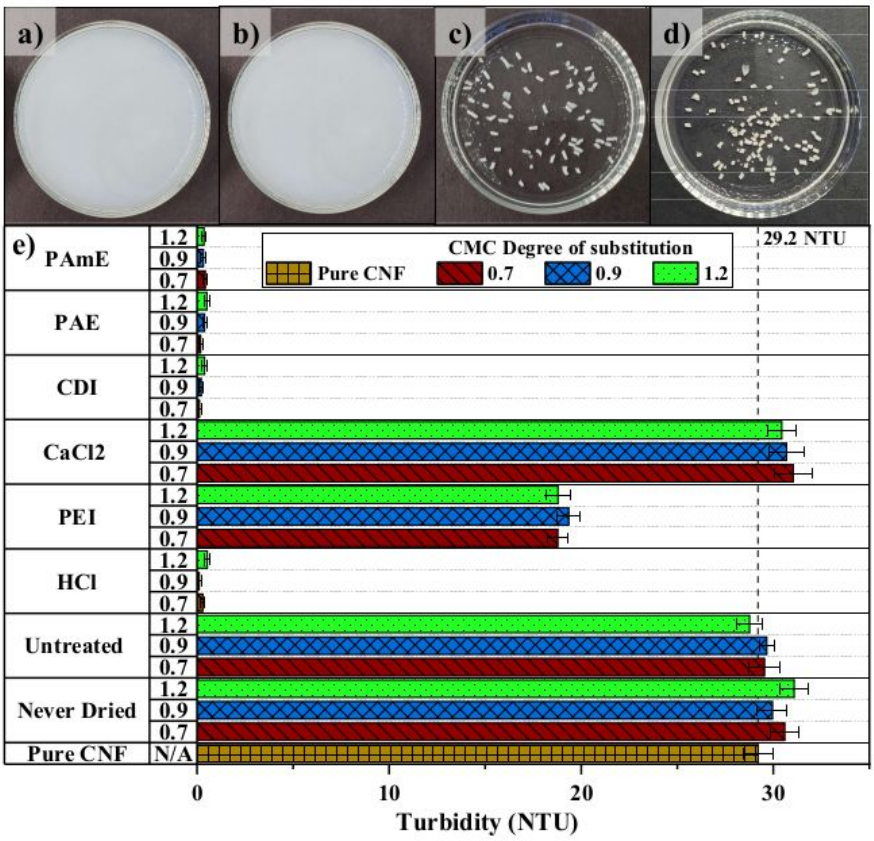

Figure 4

Dispersed never-dried CNF+CMC (a), redispersed dried-untreated CNF+CMC (b), redispersed HCl treated CNF+CMC (c), and redispersed PAE treated CNF+CMC (d) all in water after 24 hours of mechanical stirring and with a D.S. of 0.7. The turbidity response of treated and untreated CNF+CMC materials each prepared with CMC with three different degrees of substitution (D.S. = 0.7, 0.9, and 1.2) (e). Untreated, PEI, CaCl2, HCl, and CDI treated samples were dried at 70 °C while PAE, PAmE treated samples were dried at 85 °C. The CNF+CMC pellets were stirrer for 24 h in water at 25 °C before turbidity was collected and the pictures were taken. For each treatment type and D.S., a freshly prepared suspension was analyzed. Six measurements were carried out per sample. The mean and standard deviation error bars are displayed, respectively.

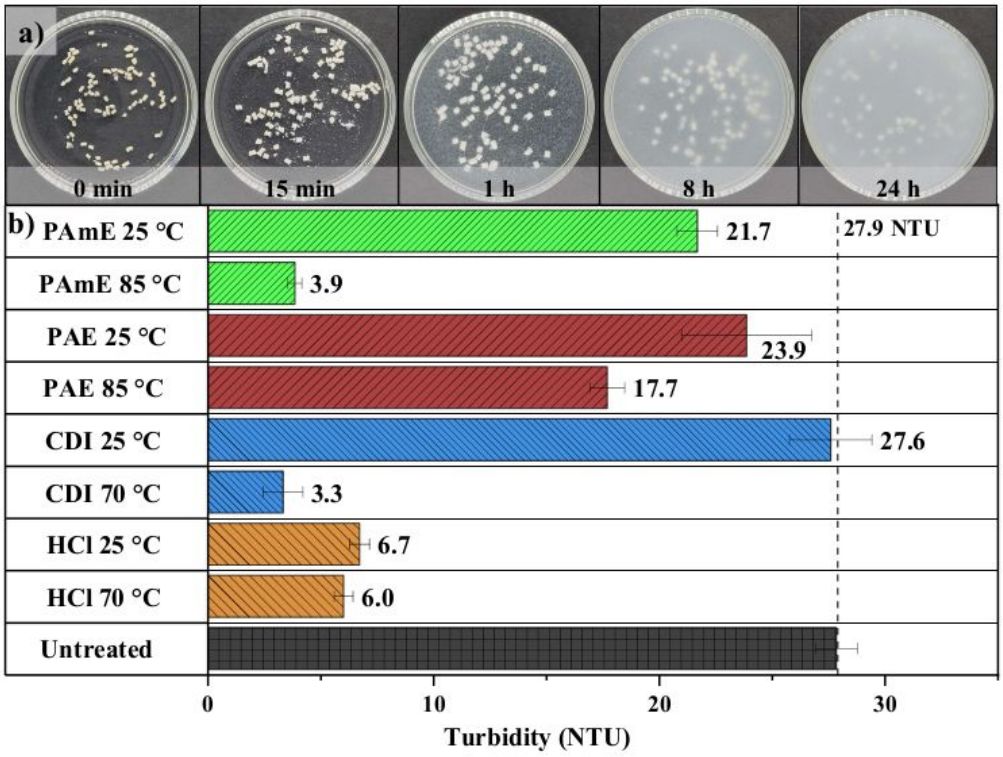

Figure 5

Redispersion behavior at different points in time for CNF+CMC treated with PAE cured at 85 °C in 0.1 M NaOH (a) and turbidity response of different treated and untreated CNF+CMC materials in 0.1 M NaOH at two curing temperatures(b). The suspensions were stirrer for 24 h before turbidity was collected. For each treatment type, two curing temperatures were evaluated while the CMC's D.S. remained constant at 0.7. A freshly prepared suspension was analyzed for each measurement. Six measurements were carried out per sample. The mean and standard deviation error bars are displayed, respectively.

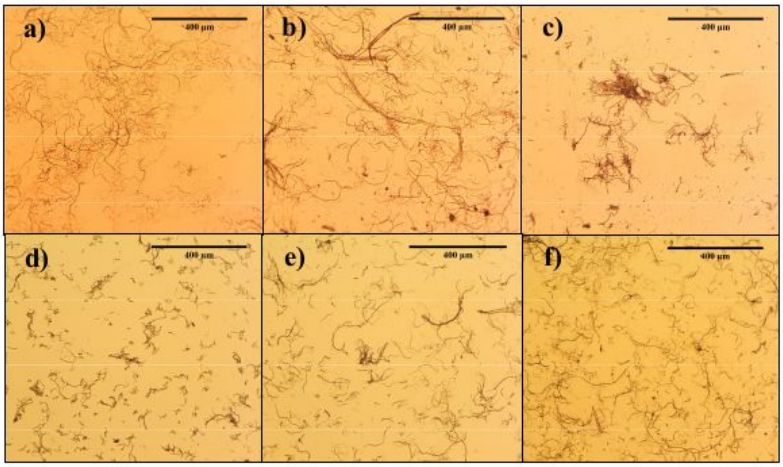

Figure 6

Optical micrographs of never-dried pure CNF dispersed in water (a), and dried-untreated CNF+CMC with a D.S. of 0.7 redispersed in water (b). Optical micrographs of CNF+CMC treated with CDI cured at 70 °C (c), CNF+CMC treated with HCl cured at 70 °C (d), CNF+CMC treated with PAE cured at 85 °C (e), and CNF+CMC treated with PAmE cured at 85 °C (f) all redispersed in 0.1 M NaOH and with a CMC D.S. of 0.7. The black scale bars in the top right have a length of 400 µm. Expanded (i.e., lower magnification) optical micrographs of the same dispersions are shown in Figure S11 and Figure S12.

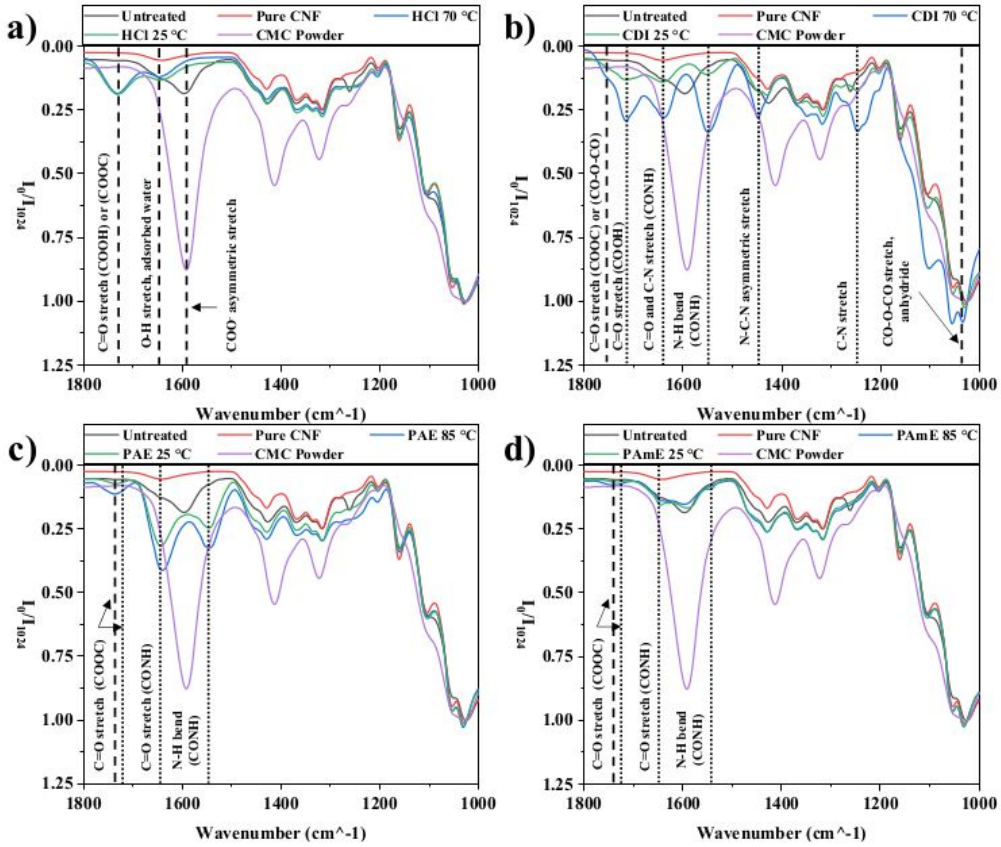

Figure 7

FTIR analysis of CNF+CMC treated with; HCl cured at 25 °C and 70 °C (a), CDI cured at 25 °C and 70 °C (b), PAE cured at 25 °C and 85 °C (c), and PAmE cured at 25 °C and 85 °C (d) all with a CMC D.S. of 0.7. The control groups of pure CNF, pure CMC powder, and untreated CNF+CMC are also shown on the respective plots. The samples were conditioned under vacuum for 24 h at room temperature before testing. All the spectra shown were baseline corrected and 20 scans were collected. All intensities were all normalized by the invariant cellulose peak intensity at 1024 cm-1. Dashed vertical lines mark the peak locations found in the treated CNF+CMC spectra while the dotted vertical lines mark peaks found in the pure compound spectra, respectively.

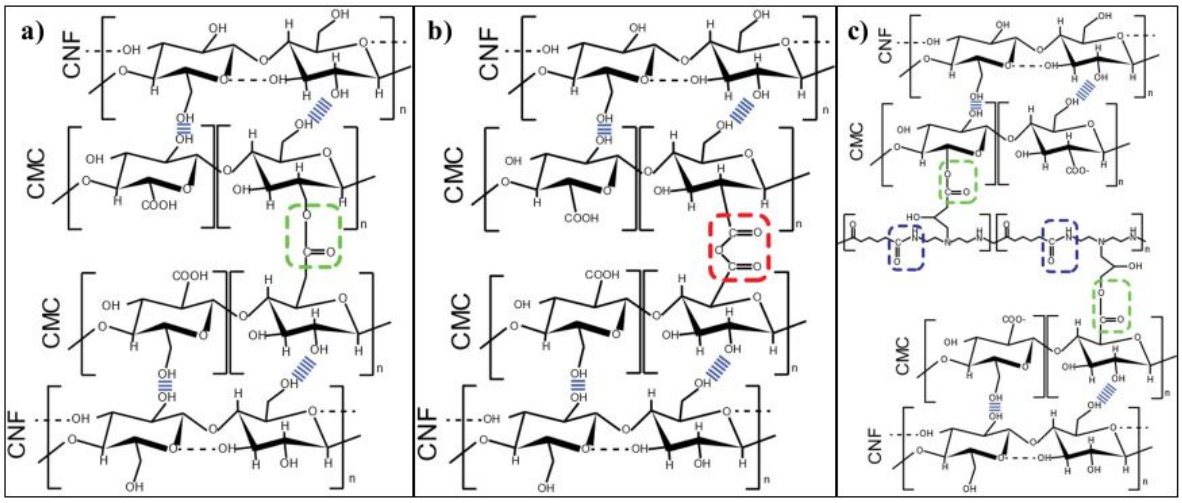

Figure 8

Schematic of CNF with adsorbed CMC through hydrogen bonding with possible ester linkages (circled in green) formed due to treatment with HCl (a), anhydride linkages (circled in red) due to treatment with CDI (b), and ester linkages (circled in green) formed due to treatment with PAE and PAmE (c). Note that amide groups (circled in blue) are present in the PAE and PAmE backbone. All the schematics shows CMC with a D.S. of 1.

Supplementary Files

This is a list of supplementary files associated with this preprint. Click to download.

- Supportinginformation.docx
- VideoS1.mp4
- VideoS2.mp4